Journal of Alloys and Compounds 509 (2011) 8567–8572

Contents lists available at ScienceDirect

Journal of Alloys and Compounds

journal homepage: www.elsevier.com/locate/jallcom

Effects of phase composition on the mechanical properties and damping capacities of as-extruded Mg–Zn–Y–Zr alloys

Jingfeng Wang[a,b,*], Shan Gao[a,b], Pengfei Song[a,b], Xuefei Huang[c], Zhangzhi Shi[c], Fusheng Pan[a]

[a] National Engineering Research Center for Magnesium Alloys, Chongqing University, Chongqing 400044, PR China
[b] College of Materials Science and Engineering, Chongqing University, Chongqing 400044, PR China
[c] Laboratory of Advanced Materials, Department of Materials Science and Engineering, Tsinghua University, Beijing 100084, PR China

ARTICLE INFO

Article history:
Received 16 January 2011
Received in revised form 2 June 2011
Accepted 6 June 2011
Available online 13 June 2011

Keywords:
Magnesium alloy
Mechanical Property
Damping
Transmission electron microscope
Long period stacking ordered phase

ABSTRACT

The present work mainly investigated the microstructures, mechanical properties, and damping capacities of as-extruded Mg–Zn–Y–Zr alloys with varied phase composition. Alloys of $MgZn_2$, W-phases ($Mg_3Y_2Zn_3$), I-phases (Mg_3YZn_6), and X-phases ($Mg_{12}YZn$) were obtained by adjusting the Zn/Y ratio (in wt%). The crystallographic structure of the X-phase [long period stacking ordered (LPSO) phase] and the crystallographic relationship between the W-phase and the Mg matrix were determined. The strengthening effects of the phase composition on the alloys exhibited the following trend: W + LPSO > LPSO>W + I > $MgZn_2$. Variations in the phase composition resulted in almost consistent variations in the damping capacities of the alloys compared with their mechanical properties. The LPSO structural phase could enhance the mechanical properties and simultaneously maintain the good damping capacity of the alloys.

1. Introduction

In modern engineering material designs, increasing attention has been paid to mechanical vibrations and undesirable noise for their negative effects on machine precision and component rupture by fatigue. Due to their low density, high specific strength, and preferable damping capacity, magnesium alloys have been regarded as promising materials for high-damping, anti-vibration, and noise-reduction applications in various areas, including the robotics, electric, automotive, and aerospace industries [1–5].

For pure magnesium, energy dissipation by dislocation movements is the major internal friction mechanism. The vibration of the dislocation loops around their equilibrium position is responsible for the very high damping level, 10 times higher than in pure aluminium [6]. As the traditional high-damping magnesium alloy, a combination of solution treatment at 550 °C for 30 min and aging at 300 °C for 16 h effectively improves the damping capacity of Mg–Zr alloy for the crucial role of twin structures in the alloy matrix [7]. Several studies have recently been conducted on the damping capacities of magnesium alloys by adding other alloying elements such as calcium and lithium. Improved damping performance of an Mg–1%Ca alloy was obtained using a low-temperature casting method, opening a new window to develop better damping performance of magnesium alloys [8]. Studies on the low-frequency damping capacities of as-extruded Mg–11.2Li–0.95Al–0.43Zn alloy revealed that the high-temperature damping background for the alloy exhibits a viscoelastic relaxation characteristic. This alloy possesses extremely low activation energy for a high-temperature damping background due to its abundant α/β phase boundaries [9]. In addition, the Mg matrix composite has been developed to obtain higher damping capacities than the commercial magnesium alloys. Compared with the AZ91 alloy, the damping capacities of the Grp/AZ91 composite extruded at 300 °C are improved significantly by the addition of graphite particles, whose Q^{-1} is increased by nearly 400% [10].

However, materials with high damping capacities generally exhibit poor mechanical properties, such as low hardness, yield stress, and tensile strength, which restrict their extensive application as anti-vibration structural components. Thus, balancing the damping capacities and mechanical properties of magnesium alloys has become a critical problem for engineering applications. The microstructure, second phase, fatigue behaviour, corrosion behaviour, and other processing techniques of Mg–Zn–Y–Zr alloys have recently drawn widespread attention because of the outstanding comprehensive mechanical properties of these alloys [11–14]. Three kinds of ternary equilibrium Mg–Y–Zn phases exist in this alloy system: the W-phase ($Mg_3Y_2Zn_3$, cubic structure), the I-phase (Mg_3YZn_6, icosahedral quasicrystal structure), and the X-phase [$Mg_{12}YZn$, long period stacking ordered (LPSO) structure] [15–18]. The W-phase basically has no strengthening effect on Mg–Zn–Y–Zr

* Corresponding author. Tel.: +86 23 65112153.
E-mail address: jfwang@cqu.edu.cn (J. Wang).

0925-8388/$ – see front matter © 2011 Elsevier B.V. All rights reserved.
doi:10.1016/j.jallcom.2011.06.017

system alloys, although there is no direct poof to support the detrimental effect of the W-phase on the mechanical properties of alloys [19]. Rigid atomic bonding between the quasicrystalline I-phase and the α-Mg matrix is important in enhancing the strength of Mg–Zn–Y–Zr alloys. Very fine grain sizes up to ~1 μm with yield strengths up to ~400 MPa in tension and compression, with elongations ranging from 12% to 18%, have recently been achieved by direct extrusion of chill casting Mg–Zn–Y alloy containing a quasicrystalline phase [20]. In addition, for the LPSO phase, the critical resolved shear stress of the basal slip was roughly estimated to be 10–30 MPa, significantly larger than that of pure magnesium (~1 MPa) or Mg–Zn solid solutions at ambient temperature [21]. The existence of the LPSO phase strongly enhances the refinement of Mg matrix grains during extrusion, which leads to a significant increase in yield stress through the Hall–Petch relationship. Moreover, the LPSO phases, which are aligned along the direction of extrusion, act as hardening phases, being roughly coordinated with the short-fibre reinforcement mechanism [22]. Therefore, the LPSO structure X-phase is another efficient strengthening phase in Mg–Zn–Y–Zr alloys.

Despite these latest findings, the comprehensive effects of variations in the phase composition of such alloys on their damping capacities were rarely studied. In the present work, the mechanical properties and damping capacities of Mg–Zn–Y–Zr alloys with varied phase compositions by tailoring the Zn/Y ratio were investigated to obtain balanced damping capacities and mechanical properties of magnesium alloys using dynamic mechanical analyser (DMA), tensile tests, scanning electron microscope (SEM), and transmission electron microscope (TEM). The present investigation hopes to contribute to the lightweight material designs of magnesium alloy for anti-vibration and noise-reduction applications.

2. Experimental details

Experimental magnesium alloys (I–IV) were prepared from commercial pure magnesium (99.95 wt%), zinc (99.95 wt%), Mg–30Zr master alloy, and Mg–25Y master alloy in an electrically resistant furnace under the protection of 0.2% SF_6 + CO_2 mixed gas. Alloy I, which had a chemical composition of Mg–6.0%Zn–0.5%Zr (wt%), was designed with properties comparable with the ZK60 alloy for its mature engineering application. The chemical composition of alloys II–IV was designed with decreasing Zn/Y ratios by increasing the content of Y and simultaneously decreasing the content of Zn. The chemical compositions of the designed alloys are listed in Table 1. The ingots were homogenised at 400 °C for 29 h, and then extruded using a 2.500 T LXJ horizontal extruder at an extrusion ratio of 25 at 450 °C extrusion temperature.

Table 1
Chemical compositions of the test alloys.

Alloy code	Nominal composition (wt%)	Actual composition (wt%)			
	$(Mg–x\%Y–0.6\%Zr)_{1-y}Zn_y$	Mg	Zn	Y	Zr
I	$x = 0, y = 6$	93.50	6.01	0	0.49
II	$x = 1, y = 6$	92.73	5.94	0.96	0.37
III	$x = 3.6, y = 6$	90.70	5.30	3.59	0.41
IV	$x = 4.7, y = 6$	90.04	4.61	4.74	0.61

The microstructures of the specimens were examined using an Olympus optical microscope. Phase analysis was performed with a Rigaku D/MAX2500PC X-ray diffractometer (XRD) using a copper target with a scanning angle from 20° to 90° and a scanning speed of 2°/min. The microstructural morphology and compound composition of the alloys were examined by VEGA II LMU SEM with energy dispersive X-ray spectrometry (EDS). The detailed microstructures of the samples were further examined by TEM (ZEISS LIBRA 200 FE) with an accelerating voltage of 200 kV. Tensile testing at ambient temperature was performed on a Shimadzu CMT-5105 material testing machine with a stretching rate of 3 mm/min. The damping samples were machined to dimensions of 45 mm × 5 mm × 1 mm parallel to the extrusion direction using an electric spark cutter. Damping capacity was determined by dynamic mechanical analysis (TA-DMA Q800) in single cantilever vibration mode at a measurement frequency of 1 Hz and various strain amplitudes (ε) ranging from 5×10^{-5} to 1×10^{-3}, as well as by the loss tangent ($\tan\varphi$). Given that $\tan\varphi$ is equivalent to the inverse quality factor (Q^{-1}) when the internal friction is very low, the damping capacities of the alloys were evaluated using Q^{-1} as a substitute for $\tan\varphi$.

3. Results and discussion

3.1. The microstructure of the as-extruded Mg–Zn–Y–Zr alloys

The microstructures of the as-extruded Mg–Zn–Y–Zr alloys are shown by the optical micrographs in Fig. 1. The grains of alloys I–IV, with average grain sizes of 14.2, 9.8, 3.7, and 2.2 μm, respectively, became much finer with increasing Y content. During solidification, the accumulation of Y in front of the solid–liquid interface induces the expansion of a constitutional supercooling area, accelerating the nucleation rate. As a surface-active element, Y can reduce the nucleation energy and the critical nucleation radius.

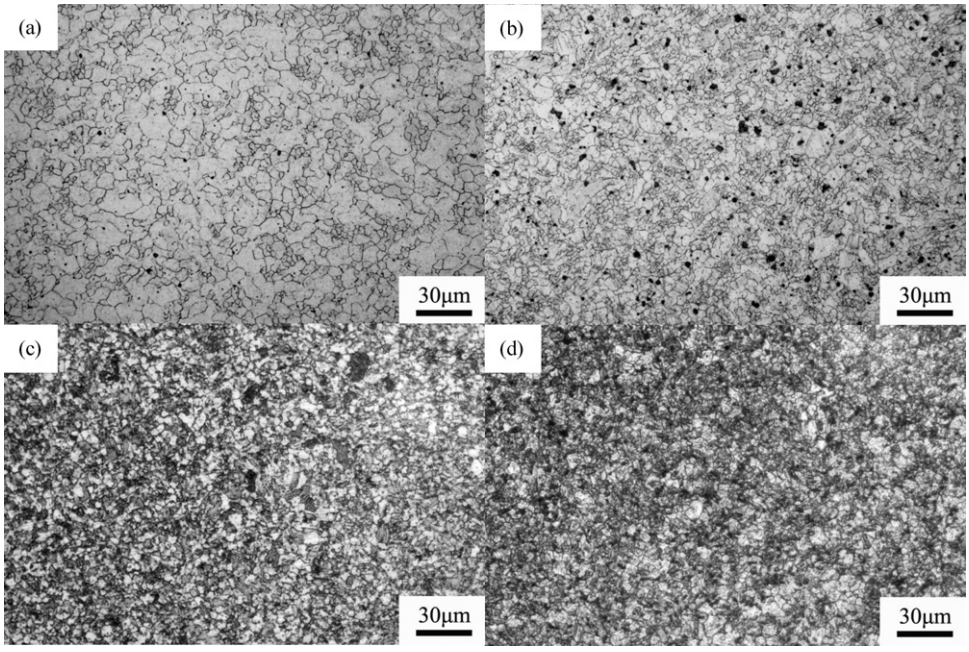

Fig. 1. Optical micrographs of as-extruded Mg–Zn–Y–Zr series magnesium alloys: (a) I; (b) II; (c) III; (d) IV.

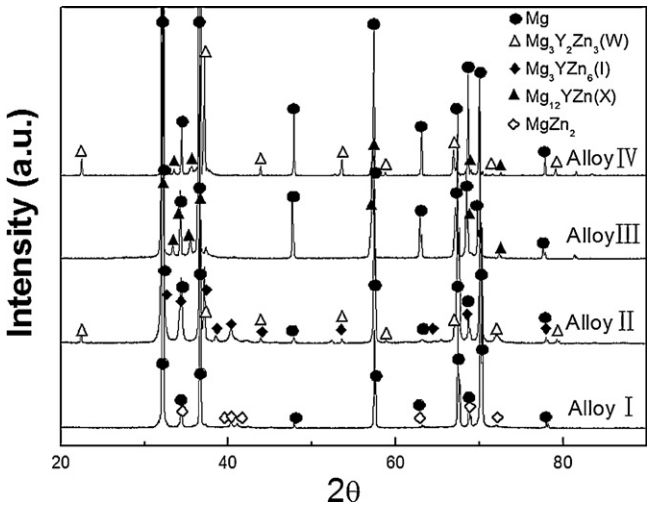

Fig. 2. XRD patterns of the as-extruded Mg–Zn–Y–Zr series magnesium alloys.

During extrusion, the addition of Y can cause ternary equilibrium Mg–Zn–Y phases to effectively restrain grain growth during dynamic recrystallization. Y-free alloy I was observed to retain few recrystallised grains among coarse primary crystals. Y-containing alloys II–IV mainly featured fine recrystallised grains and almost no recrystallised grain growth coarsening. Several other studies have reported on the grain refinement effects of Y in Mg alloys [23,24]. Therefore, the addition of Y can effectively refine the crystal grains of as-extruded Mg–Zn–Y–Zr alloys. The Zr particle acts as a nucleus during solidification and is able to increase the speed of nucleation.

Granular black precipitations were mainly distributed in the grain boundaries of alloy I. After the addition of Y to alloy II, larger and more granular black precipitations in the grain boundaries were produced. With decreasing Zn/Y ratio, alloy III showed additional bulk-shaped precipitations along its grain boundaries. Sufficient amounts of Zn and Y solid solution atoms in the Mg matrix of alloy IV resulted in the precipitation of various-sized secondary granular phases, aside from bulk-shaped precipitations along its grain boundaries. These secondary phases displayed inhomogeneous and dispersive precipitation morphologies.

XRD analysis revealed the main phases of the alloys according to their variations in Zn and Y content (Fig. 2). Five main phases were observed, namely, the α-Mg matrix, $MgZn_2$, the W-phase ($Mg_3Y_2Zn_3$), the I-phase (Mg_3YZn_6), and the X-phase ($Mg_{12}YZn$). The phase compositions of the different alloys are listed in Table 2.

Although the W-phase, which has an fcc structure, is quite common in Mg–Zn–Y–Zr alloys, this phase is generally not considered an effective strengthening phase [25,26]. The I-phase, which has a quasicrystal structure, showed efficient strengthening effects for numerous desirable properties, such as hardness, thermal stability, high corrosion resistance, low coefficient of friction, and low interfacial energy, among others [27,28]. Thus, the I-phase is sufficiently stable to restrain grain coarsening during hot extrusion, especially when the quasicrystals exist in the α-Mg matrix as a second phase in Mg–Zn–Y–Zr alloys. The thermal stability and low interfacial energy between the quasicrystals and the α-Mg matrix provide strong bonding properties at the interface between the I-phase and the matrix. The stable LPSO-phase with $Mg_{12}YZn$ was discovered during investigations of the Mg–Y–Zn ternary phase diagram around the magnesium corner, and was named X-phase by Padezhnova et al. [29]. At a Zn/Y ratio of 0.98, alloy IV comprised the α-Mg matrix, as well as the W- and X-phases. According to a research on the solidification pathways and constituent phases of Mg–Zn–Y–Zr alloys, the main phases of a ZW66 alloy with a Zn/Y ratio of 0.85 include the α-Mg and W- and X-phases [15]. Therefore, the X- and W-phases are more easily obtained in Mg–Zn–Y–Zr alloys when Zn and Y have approximately the same mass fractions. Further confirmations of the secondary phases in alloy IV were performed via TEM.

Table 2
Phase compositions in Mg–Zn–Y–Zr series magnesium alloys.

Alloy code	Zn/Y	Phase composition
I	–	α-Mg + $MgZn_2$
II	6.19	α-Mg + W-$Mg_3Y_2Zn_3$ + I-Mg_3YZn_6
III	1.48	α-Mg + X-$Mg_{12}YZn$
IV	0.98	α-Mg + W-$Mg_3Y_2Zn_3$ + X-$Mg_{12}YZn$

Fig. 3(a) and (b) shows the TEM image and corresponding selected area electron diffraction (SAED) pattern of the as-extruded alloy IV. In Fig. 3(a), the bright area indicates the α-Mg matrix while the dark area shows the LPSO structure X-phase with a zonal axis of $[2\bar{1}\bar{1}0]_{LPSO}$, whose stacking orientation is parallel to the $[0\,0\,0\,1]_\alpha$ direction of the α-Mg matrix. Fourteen consistent diffraction spots with an LPSO structure were noted at regular intervals between the transmission and diffraction spots corresponding to the {0 0 0 2} plane of the Mg matrix in the SAED pattern of Fig. 3(b).

The structure of the X-phase $Mg_{12}YZn$ has long been assumed to be an 18R structure in the Mg–Zn–Y system. However, the metastable 18R structure is often gradually replaced by the 14H structure during prolonged heat treatment or processing. Thus, the 14H phase appears to be a thermodynamically stable equilibrium phase in the Mg–Zn–Y system. Furthermore, a previous study has reported [30] that this 14H unit cell is hexagonal in shape with lattice parameters $a = 1.11$ nm and $c = 3.65$ nm. The stacking sequence of this cell is ABABCACACACBABA, and contains two twin-related building blocks with opposite shears in an ABCA-type plane-stacking sequence. From the TEM images, along with the XRD results, the X-phase was found to possess a 14-layer period stacking structure.

Fig. 3(c) and (d) show the TEM image of the W-phase and its corresponding SAED pattern in the as-extruded alloy IV, revealing the orientation between the W-phase and the Mg matrix. The structure of the W-$Mg_3Y_2Zn_3$ phase, as determined by Padezhnova et al. [29] using XRD, possesses a partially ordered $AlMnCu_2$-type fcc structure with $a = 0.6848$ nm. The space group of this phase is $Fm\bar{3}m$. Fig. 3(d) shows the diffraction spot in the SAED pattern of the matrix and the W-phase, indicating the existence of a rational orientation between the W-phase and the matrix, that is, the zonal axis $[0\,0\,1]_W$ is parallel to the zonal axis $[0\,1\,\bar{1}\,0]_\alpha$, and $(2\,2\,0)_W$ is parallel to $(0\,0\,0\,2)_\alpha$. Thus, the orientation between the W-phase and the matrix can be expressed as $[0\,0\,1]_W//[0\,1\,\bar{1}\,0]_\alpha$, $(1\,1\,0)_W//(0\,0\,0\,1)_\alpha$, which is different from that previously reported ($[0\,0\,1]_W//[\bar{2}\,1\,1\,0]_\alpha$, $(1\,1\,0)_W//(0\,0\,0\,1)_\alpha$) [31]. Considering that the morphology of the secondary phase is dependent not only on the interfacial energy during solidification, only multiple interfaces with curved features exist between the matrix and the W-phase along the zonal axis $[0\,1\,\bar{1}\,0]_\alpha$ of the matrix, not straight ones. The atomic bonding between the W-phase and the Mg matrix is very weak due to the limited symmetry of the crystal lattice of the W-phase structure and the incoherence of the interface between them [32,33].

3.2. Mechanical properties of the as-extruded Mg–Zn–Y–Zr alloys

The mechanical properties of as-extruded Mg–Zn–Y–Zr alloys were compared (Fig. 4). The strength and elongation of the alloys markedly increased with decreasing Zn/Y ratio. Alloy IV exhibited the highest ultimate tensile (345 MPa) and yield (323 MPa) strengths. Alloy II had the best plasticity with 22.3% elongation, whereas alloy III exhibited excellent comprehensive mechanical

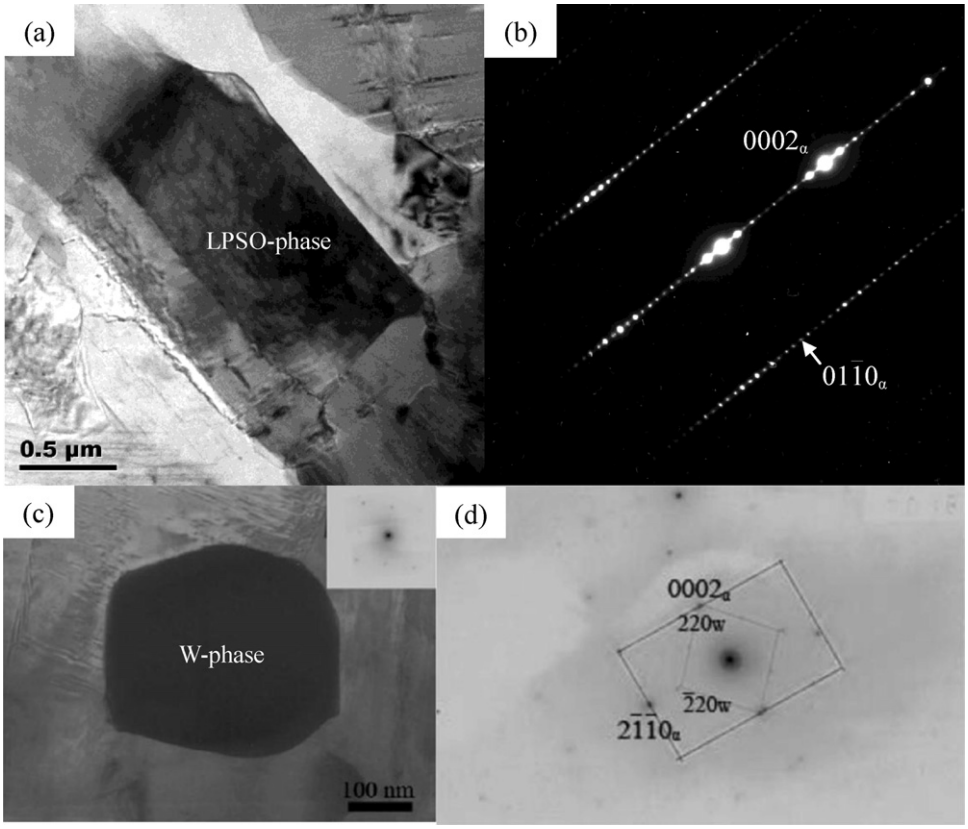

Fig. 3. TEM images of the LPSO phase (a) and its corresponding selected area electron diffraction (SAED) pattern, (b) recorded along the $< 2\bar{1}\bar{1}0>_\alpha$ direction, and the W-phase, (c) and its corresponding SAED pattern, (d) recorded along the $< 01\bar{1}0>_\alpha$ direction in alloy IV.

properties with an ultimate tensile strength of 330 MPa, yield strength of 292 MPa, and 20.7% elongation. Given that the four alloys correspond to four phase compositions, the phase strengthening efficiency followed the trend W + LPSO (alloy IV) > LPSO (alloy III) > W + I (alloy II) > $MgZn_2$ (alloy I). In comparison, the phase toughening efficiency followed the trend W + I (alloy II) > LPSO (alloy III) > $MgZn_2$ (alloy I) > W + LPSO (alloy IV).

From these results, the LPSO and quasicrystal structural phases have conspicuous strengthening effects on the mechanical properties of the alloys, particularly on their yield strength. The strengthening effects of the LPSO structure X-phase on the Mg–Zn–Y–Zr alloys are more efficient than those of the quasicrystal structural phase. However, the quasicrystal structural phase can

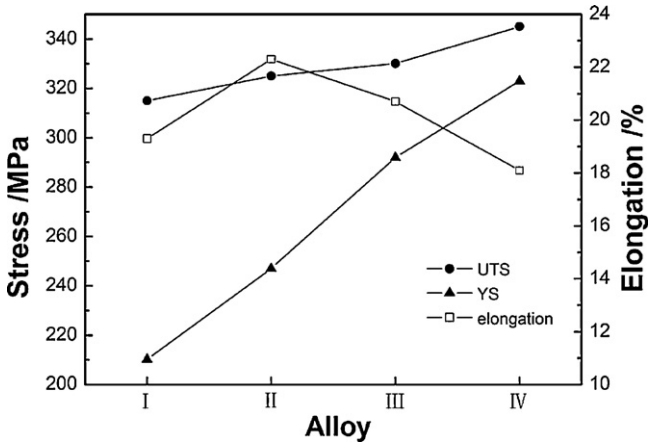

Fig. 4. Mechanical properties of as-extruded Mg–Zn–Y–Zr series magnesium alloys.

better preserve plasticity in the alloys. A previous report [34] has noted that a stable coherent interface between the LPSO phase and the α-Mg matrix does not favour nucleation sites for voids and/or microcracks during deformation, which are important for the strength and ductility of the alloy. Large LPSO blocks could transform into small kink bands due to kinking, resulting in refinement, rather than coarsening, of the LPSO phase. According to the Hall–Petch relationship, refined kinking can result in a corresponding hardening of the LPSO region. Adjacent kink grain boundaries in the Mg matrix could also slide to accommodate high-angle kink boundaries in the LPSO phase without intergranular cracking, thereby relaxing large local strains and leading to relatively homogeneous plastic deformation. Thus, aside from LPSO phase – Mg matrix interfacial strengthening, LPSO structural kinking could also contribute to the strengthening and toughening of the alloy. Although the W-phase is generally not considered as a very effective strengthening phase, the diffusive distribution of the W-phase in the α-Mg matrix after hot extrusion can also pin the dislocation and contribute some dispersion-strengthening to the alloys. Due to the interface layer with a 3–5 nm thickness of the α-Mg matrix preserving the orientation relationship with the I-phase and the coherency between the I-phase and the α-Mg matrix achieved by introducing steps and ledges periodically along the interface [35], the atomic bonding between the I-phase and the hexagonal structure is rigid enough to be retained during severe plastic deformation of alloy II. Generally, elongation tends to be low for an alloy containing a large number of intermetallic particles because dislocations are formed in the region surrounding the hard particles, resulting in decohesion from the matrix [36]. Debonding or microscale defects at the particle/matrix interface are restrained due to the stable and coherent interface between the matrix and the I-phase. These conditions indicate the best plasticity and high

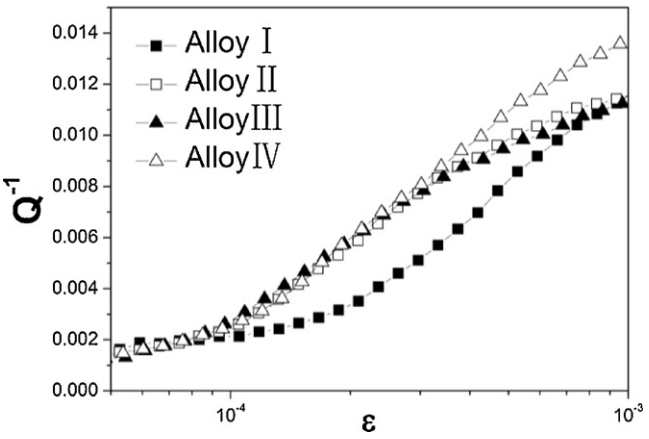

Fig. 5. Damping-strain amplitude curves of as-extruded Mg–Zn–Y–Zr series magnesium alloys under ε ranging from 5×10^{-5} to 1×10^{-3}.

strength of alloy II. Therefore, the LPSO structure X-phase provides more effective strengthening effects to the Mg–Zn–Y–Zr alloys, whereas the quasicrystal structure I-phase can better preserve the plasticity of these alloys.

3.3. Damping capacities of the as-extruded Mg–Zn–Y–Zr alloys

The variations in damping capacities corresponding to alloys with different phase compositions were also investigated in terms of the enhancement in mechanical properties of the alloys. Fig. 5(a) shows the damping capacities as a function of the strain amplitude of the alloys at room temperature. Q^{-1} values for all alloys continuously increased with increasing strain amplitude. No evident variation was observed among the alloys at low strain amplitudes. Once the strain amplitude exceeded a critical value, however, the damping of alloys II–IV was conspicuously better than that of the Y-free alloy I. The critical strain amplitudes of alloys II–IV were evidently higher than that of the Y-free alloy due to the presence of Y. With further increase in strain amplitude, the damping capacity of alloy IV became evidently better than those of the other alloys. The damping capacities of the four alloys showed the following trend: W + LPSO (alloy IV) > LPSO (alloy III) > W + I (alloy II) > $MgZn_2$ (alloy I). This trend approximates the strengthening efficiency of the mechanical properties.

The damping capacities of magnesium and magnesium alloys are reported to be dependent on the strain amplitude, and are considered to be related to the dislocation movement on the basal planes [37–39]. At low strain amplitudes and slight alternating stress, mobile dislocations are pinned by the pinning point and bow back and forth between neighbouring weak pinning points with short distances, generating low internal friction in the alloys. At high strain amplitudes, the additional stress becomes critically high such that the dislocations break away at weak points. When the stress is unloaded, the dislocation loops shrink elastically and are finally pinned by point defects. During unpinning and the rebound of dislocation loops, static hysteretic internal friction is produced, specifically, strain-dependent damping generated at the high strain amplitude region. Q^{-1} of alloy I was obviously higher than those of alloys II–IV under the strain amplitude exceeding the critical value. Due to the presence of Y in the alloys, a mass of ternary equilibrium Mg–Zn–Y phases precipitating from the α-Mg matrix results in decreased amounts of solute atoms in the α-Mg matrix. The decreased amounts of solute atoms as weak pinning points could increase the length between weak pinning points, increasing static hysteretic internal friction produced by the unpinning and the rebound of dislocation loops. On the other hand, in terms of phase composition, alloys II and IV with W-phases have better damping capacities, which can be attributed to the incoherence of the interface between the W-phase and the Mg matrix. Due to the weak atomic bonding between the W-phase and the Mg matrix, mobile dislocations are likely to be generated and moved, which can positively affect the internal frictions of the alloys. The coherence of the α-Mg/I-phase interface and the stable lattice structure were not beneficial to the generation and movement of the dislocation and are considered disadvantages for the damping capacities of alloy II. Although the LPSO structural X-phase also exhibits the coherence of the α-Mg/LPSO-phase interface, which resembles the I-phase, the back and forth movement of the stacking faults to comply with the vibrational stress at a high strain amplitude [40] in the LPSO-phase can contribute to the internal friction of alloy IV. Thus, Q^{-1} of alloy IV is higher than those of the other alloys at higher strain amplitude.

4. Conclusions

(1) Alloys with varied phase composition, including $MgZn_2$, W-phase ($Mg_3Y_2Zn_3$), I-phase (Mg_3YZn_6), and X-phase ($Mg_{12}YZn$), may be obtained by adjusting the Zn/Y ratios of Mg–Zn–Y–Zr alloys. Analyses of the LPSO- and W-phases in alloy IV indicate that the LPSO-phase with a 14-layer period stacking structure is the X-phase ($Mg_{12}YZn$), and that the W-phase has a new orientation in relation to the α-Mg matrix. This orientation can be expressed as $[0\,0\,0\,1]_W//[0\,1\,\bar{1}\,0]_\alpha$, $(1\,1\,0)_W//(0\,0\,0\,1)_\alpha$.

(2) The phase strengthening efficiency follows the trend W + LPSO (alloy IV) > LPSO (alloy III) > W + I (alloy II) > $MgZn_2$ (alloy I), whereas the phase toughening efficiency follows the trend W + I (alloy II) > LPSO (alloy III) > $MgZn_2$ (alloy I) > W + LPSO (alloy IV). These trends indicate that the LPSO phase provides more efficient strengthening effects to the alloys, whereas the I-phase provides more efficient toughening effects.

(3) The damping capacities of the four alloys exhibit the following trend: W + LPSO (alloy IV) > LPSO (alloy III) > W + I (alloy II) > $MgZn_2$ (alloy I). This trend indicates that the LPSO phase could enhance the mechanical properties of the Mg–Zn–Y–Zr alloys and simultaneously optimise their damping capacities.

Acknowledgements

The authors are grateful for the financial support from Joint Foundation, National Natural Science Foundation Commission of China and China Academy of Engineering Physics (grant no. 10876045), National Basic Research Program of China (grant no. 2007CB613704), National Key Technology R&D Program (project no. 2011BAE22B04) and National Natural Science Foundation of China (project no. 50725413).

References

[1] S.H. Chang, S.K. Wu, W.L. Tsai, J.Y. Wang, J. Alloys Compd. 487 (2009) 142–145.
[2] D.Q. Wan, J.C. Wang, G.C. Yang, Mater. Sci. Eng. A 517 (2009) 114–117.
[3] L.H. Liao, X.Q. Zhang, H.W. Wang, X.F. Li, N.H. Ma, J. Alloys Compd. 429 (2007) 163–166.
[4] R. Schaller, J. Alloys Compd. 355 (2003) 131–135.
[5] K. Nishiyama, R. Matsui, Y. Ikeda, S. Niwa, T. Sakaguchi, J. Alloys Compd. 355 (2003) 22–25.
[6] S.M. Seyed Reihani, C. Esnouf, G. Fantozzi, G. Revel, J. Phys. 42 (1981) C5–C145.
[7] M.H. Tsai, M.S. Chen, L.H. Lin, M.H. Lin, C.Z. Wu, K.L. Ou, C.H. Yu, J. Alloys Compd. 509 (2011) 813–819.
[8] D.Q. Wan, Mater. Charact. 62 (2011) 8–11.
[9] S.K. Wu, S.H. Chang, W.L. Tsia, H.Y. Bor, Mater. Sci. Eng. A (2011), doi:10.1016/j.msea.2011.04.047.
[10] Y.W. Wu, K. Wu, K.K. Deng, K.B. Nie, X.J. Wang, X.S. Hu, M.Y. Zheng, J. Alloys Compd. 506 (2010) 688–692.
[11] S.W. Xu, M.Y. Zheng, S. Kamado, K. Wu, G.J. Wang, X.Y. Lv, Mater. Sci. Eng. A 528 (2011) 4055–4067.
[12] W.N. Tang, R.S. Chen, J. Zhou, E.H. Han, Mater. Sci. Eng. A 499 (2009) 404–410.

[13] Y. Song, D. Shan, R. Chen, E.H. Han, Corros. Sci. 52 (2010) 1830–1837.
[14] Q. Yang, B.L. Xiao, Z.Y. Ma, Scr. Mater. (2011), doi:10.1016/j.scriptamat.2011.04.041.
[15] Z.H Huang, S.M. Liang, R.S. Chen, E.H. Han, J. Alloys Compd. 468 (2009) 170–178.
[16] D.K. Xu, L. Liu, Y.B. Xu, E.H. Han, Acta Mater. 56 (2008) 985–994.
[17] D.K. Xu, W.N. Tang, L. Liu, Y.B. Xu, E.H. Han, J. Alloys Compd. 461 (2008) 248–252.
[18] A. Müller, G. Garcés, P. Pérez, P. Adeva, J. Alloys Compd. 443 (2007) L1–L5.
[19] D.K. Xu, W.N. Tang, L. Liu, Y.B. Xu, E.H. Han, J. Alloys Compd. 432 (2007) 129–134.
[20] A. Singh, Y. Osawa, H. Somekawa, T. Mukai, Scr. Mater 64 (2011) 661–664.
[21] K. Hagihara, N. Yokotani, Y. Umakoshi, Intermetallics 18 (2010) 267–276.
[22] K. Hagihara, A. Kinoshita, Y. Sugino, M. Yamasaki, Y. Kawamura, H.Y. Yasuda, Y. Umakoshi, Acta Mater. 58 (2010) 6282–6293.
[23] C.J. Ma, M.P. Liu, G.H. Wu, W.J. Ding, Y.P. Zhu, Mater. Sci. Eng. A 349 (2003) 207–212.
[24] H.S. David, Q. Ma, A.E. Mark, C. Peng, H. Zoe, Metall. Mater. Trans. A 36 (2005) 1679–1699.
[25] D.K. Xu, L. Liu, Y.B. Xu, E.H. Han, J. Alloys Compd. 426 (2006) 155–161.
[26] Z.P. Luo, S.Q. Zhang, J. Mater. Sci. Lett. 12 (1993) 1490–1492.
[27] J.M. Dubois, P. Plaindoux, E. Berlin-Ferre, N. Tamura, D.J. Sordelet, Proceedings of the Sixth International Conference on Quasicrystals, in: World Scientific, Singapore, 1997.
[28] F.S. Pierce, S.J. Poon, Q. Guo, Science 261 (1993) 737.
[29] E.M. Padezhnova, E.V. Mel'nik, R.A. Miliyevskiy, T.V. Dobatkina, V.V. Kinzhibalo, Russ. Metall. (Metally) 4 (1982) 185–188 (English Translation).
[30] Y.M. Zhu, A.J. Morton, J.F. Nie, Acta Mater. 58 (2010) 2936–2947.
[31] A. Singh, M. Watanabe, A. Kato, Mater. Sci. Eng. A 397 (2005) 22–34.
[32] A. Niikura, A.P. Tsai, A. Inoue, T. Masumoto, Philos. Mag. Lett. 69 (1994) 351.
[33] A. Singh, A.P. Tsai, Scr. Mater. 49 (2003) 143.
[34] X.H. Shao, Z.Q. Yang, X.L. Ma, Acta Mater. 58 (2010) 4760–4771.
[35] D.H. Bae, S.H. Kim, D.H. Kim, W.T. Kim, Acta Mater. 50 (2002) 2343.
[36] T.H. Courtney, Mechanical Behavior of Materials, McGraw-Hill, New York, 2000.
[37] O.A. Lamibri, W. Riehemann, Z. Trojanová, Scr. Mater. 45 (2001) 1365–1371.
[38] A.S.M.F. Chowdhury, D. Mari, R. Schaller, Compos. Sci. Technol. 70 (2010) 136–142.
[39] S.K. Wu, S.H. Chang, T.Y. Chou, S. Tong, J. Alloys Compd. 465 (2008) 210–215.
[40] B.M. Girish, B.M. Satish, K. Mahesh, Mater. Des. 31 (2010) 2163–2166.